Surface Rupturing Earthquakes of the Greater Caucasus Frontal Thrusts, Azerbaijan

Ian Pierce[1]

Ibrahim Guliyev[2]

Gurban Yetirmishli[3]

Rauf Muradov[3]

Sabina Kazimova[3]

Rashid Javanshir[1,2]

Ben Johnson[1]

Neill Marshall[1]

Richard Walker[1]

Paul Wordsworth[1]

[1] University of Oxford, 3 S Parks Road, Oxford, United Kingdom OX13AN

[2] Azerbaijan National Academy of Science, Baku, Azerbaijan

[3] Republican Seismic Survey Center of Azerbaijan National Academy of Science, Baku, Azerbaijan

Corresponding author: Ian Pierce (ian.pierce@earth.ox.ac.uk)

Key Points:

- A paleoseismic trench near Agsu, Azerbaijan provides evidence of two surface rupturing events since medieval times.
- These events occurred AD 1713-1895 and 1872-2003, and may correspond to historical earthquakes that destroyed Shamakhi in 1668 and 1902.
- Maximum shortening and dip-slip rates of the frontal thrust sheet in the eastern Kura fold-thrust belt are 8 and 8.5 mm/yr, respectively.

Abstract

Quaternary convergence at rates of ~10 mm/yr between the Arabian and Eurasian plates is largely accommodated by the Kura fold-thrust belt at the longitude of the Greater Caucasus Mountains in Azerbaijan and eastern Georgia. Here we present the results of the first paleoseismic study of the Kura fold-thrust belt in Azerbaijan. A single paleoseismic trench was excavated across a 2-m-high fault scarp near Agsu revealing evidence of two recent surface rupturing earthquakes. Radiocarbon dating of the faulted sediments places limits of earthquake timing of AD 1713-1895 and AD 1872-2003 for the two events. Allowing for uncertainties in radiocarbon dating, the two events likely correspond to historical destructive M~7 earthquakes near Shamakhi, Azerbaijan in AD 1668 and 1902. Holocene shortening and dip-slip rates for the Kura fold-thrust belt are 8 and 8.5 mm/yr, respectively, based on the depositional age of an abandoned uplifted strath terrace in a water gap to the west of Agsu. These rates should be treated as maxima, as they are ~100% of the previously determined structurally and geodetically measured shortening across the belt, and were measured from only one of two primary structures in this part of the belt. The lack of reported historical ruptures from the past 8 centuries to the west of Agsu, in contrast with the numerous recorded destructive earthquakes of the Shamakhi region, suggests that the central and western parts of the Kura fold-thrust belt produce less frequent, but more destructive earthquakes, and may have accumulated sufficient strain to produce a M>8 earthquake.

Plain Language Summary

The Greater Caucasus Mountains stretching between the Black and Caspian Seas are a result of the northward subduction of the Arabian plate beneath Eurasia. For the last 2 million years, most of this plate motion has been accommodated by the Kura fold-thrust belt in Azerbaijan & eastern Georgia. This plate motion produces periodic large earthquakes. Here a paleoseismic trenching investigation revealed evidence of two large earthquakes in the eastern part of the Kura fold-thrust belt. These earthquakes likely correspond to known historical earthquakes in 1668 and 1902. A lack of historical earthquakes to the west of this study area suggests that the rest of the Kura fold-thrust belt may produce less frequent, but more devastating earthquakes along this plate boundary.

1 Introduction

The Greater Caucasus Mountains stretch for 900 km between the Black and Caspian Seas (**Figure 1**). The Greater Caucasus have been uplifted since ~5 Ma as a result of the northeast-directed subduction of the Arabian plate beneath the Eurasian plate (Avdeev and Niemi, 2011; Cowgill et al., 2016; Forte et al., 2015; Gunnels et al., 2021; Jackson et al., 2002; Kangarli et al., 2018; McKenzie, 1972; Mumladze et al., 2015; Philip et al., 1989). This subduction has been largely accommodated by the north-dipping Main Caucasus Thrust Fault, and since ~1.5 Ma via the foreland Kura fold-thrust belt, at an average rate of 6.7-13.6 mm/yr, measured from restored balanced cross sections (Forte et al., 2013; Kangarli et al., 2018; Mosar et al., 2010), or ~10 mm/yr measured by GPS across the Kura basin (Kadirov et al., 2012; Reilinger et al., 2006; Yetirmishli et al., 2022).

The Kura fold-thrust belt extends roughly west-east for ~275 km from near Tbilisi, Georgia to near Shamakhi, Azerbaijan (**Figure 1**). The belt forms an imbricate pattern that varies along strike with between one and four thrust sheets reaching the surface. Historical destructive earthquakes in the region are well known from AD 1139, 1668, and 1828-1902 (Ismail-Zadeh et al., 2020). The 1668 and 1828-1902 events all occurred near Shamakhi (**Figure 1**), in the easternmost part of the Kura fold-thrust belt. Despite the seismic history of the region, we are aware of no prior neotectonic or paleoseismic studies that have been conducted on the faults within the Kura fold-thrust belt, nor anywhere within Azerbaijan, so the source faults of these historical earthquakes remain unknown. Jackson and Ambraseys (1997) demonstrate that historical seismicity over the past 400 years accounts for only 25% of shortening in the Caucasus. This leads to great uncertainty in the seismogenic potential of the faults in this region as it is unclear whether the lack of historical seismicity to the west of Shamaki is a result of either (a) a lapse of historical record keeping, (b) aseismic deformation (e.g. fault creep), or (c) unreleased moment that is accumulating in the Kura fold-thrust system.

Thus, investigating the paleoseismic history of the faults in the Kura fold-thrust belt is critical for understanding the seismic potential and behavior of the faults in this region. In this paper we present the results of the first paleoseismic trench investigation and a slip rate estimate from the Kura fold-thrust belt in Azerbaijan. We then provide a brief discussion on the significance of these results and place them in the context of the historical catalog.

Figure 1. (Following page) Overview map of (A) Azerbaijan showing GPS velocities relative to stable Eurasia (Kadirov, 2012), and focal mechanisms of earthquakes from the gCMT and gWFM catalogues with ISC-EHB hypocentres from 1976-present. (B) is the eastern part of the Kura fold-thrust belt showing major faults (black lines, dashed where approximate) and figure locations. The Kura fold-thrust belt has accommodated >80% of the shortening between the Lesser Caucasus and Greater Caucasus since ~1.5 Ma, at an average rate of ~7-14 mm/yr (Forte et al., 2013). Yellow lines are MMI scale isoseismals of the 1902 Shamakhi earthquake adapted from Weber (1902). Inset simplifies major regional tectonic faults and representative GPS velocity relative to stable Eurasia.

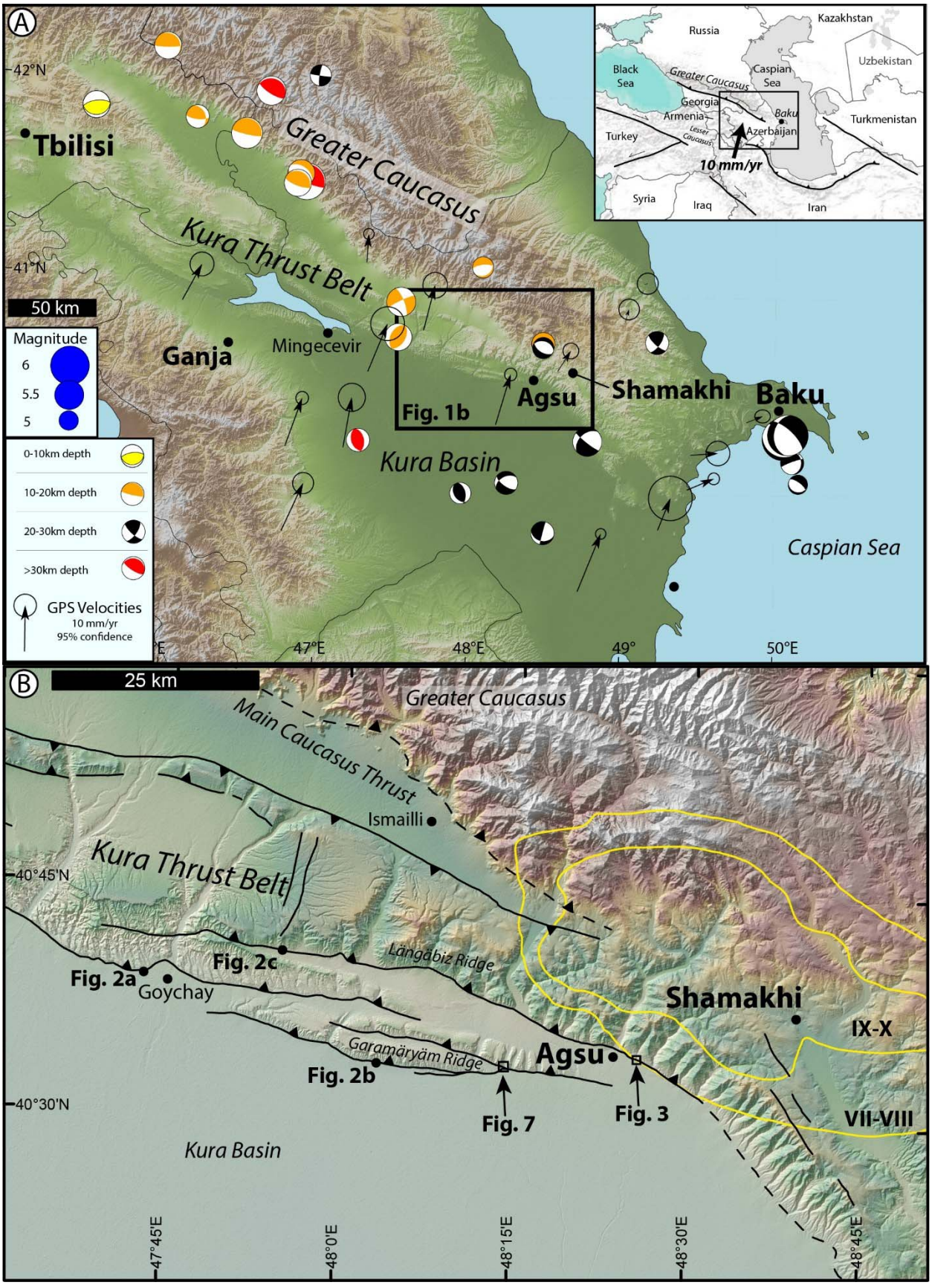
A
42°N
41°N
Tbilisi
Greater Caucasus
Kura Thrust Belt
50 km
Magnitude
6
5.5
5
Ganja
Mingecevir
Fig. 1b
Agsu
Shamakhi
Baku
Kura Basin
Caspian Sea
0-10km depth
10-20km depth
20-30km depth
>30km depth
GPS Velocities
10 mm/yr
95% confidence
47°E
48°E
49°
50°E
Russia
Kazakhstan
Uzbekistan
Black Sea
Caspian Sea
Greater Caucasus
Georgia
Armenia
Baku
Azerbaijan
Turkmenistan
Turkey
Lesser Caucasus
10 mm/yr
Syria
Iraq
Iran
B
25 km
Greater Caucasus
Main Caucasus Thrust
Ismailli
Kura Thrust Belt
40°45'N
Fig. 2a
Goychay
Fig. 2c
Längäbiz Ridge
Shamakhi
IX-X
Garamäryäm Ridge
Agsu
Fig. 2b
Fig. 7
Fig. 3
VII-VIII
40°30'N
Kura Basin
47°45'E
48°0'E
48°15'E
48°30'E
48°45'E

102

2 Methods

2.1 Fault Mapping, Photogrammetry, and Paleoseismic Trenching

Faults were remotely mapped using Google Earth, prior to field reconnaissance mapping in the spring of 2022. Key study sites were then surveyed in high detail with photogrammetry using images captured with a Teokit-equipped DJI Phantom 4 Pro v2 drone. The Teokit is a dGPS used for acquiring precise photo locations that are then corrected to an Emlid Reach RS2 dGPS base station (e.g., Zhang et al., 2019). The resulting photographs were processed using Agisoft Metashape software into DEMs and Orthomosaics, with resolutions of 6-10 and 3-5 cm/pixel, respectively (see Data Availability statement for access).

A single paleoseismic trench was excavated, cleaned, gridded, and logged. As a base for logging, an orthophoto mosaic was constructed using Agisoft Metashape software with photographs captured with a Samsung Galaxy S20 Ultra. The orthophoto was accurately scaled and oriented using reference points extracted from an iPad-lidar scan of the trench wall (**Pierce and Koehler, 2022 *in press***). Logging was then conducted on an iPad. Units and faults were divided and described following standard paleoseismic methods (e.g., McCalpin, 2009), including sedimentary facies, cross-cutting relations, and development of soils. Radiocarbon samples of charcoal, plant material, and soil were processed and analyzed at Beta Analytic laboratory in Miami, Florida, and calibrated using OxCal v4.4 (Bronk Ramsey, 1995) with the IntCal20 calibration curve. Ages and processing details are listed in **Table 1**.

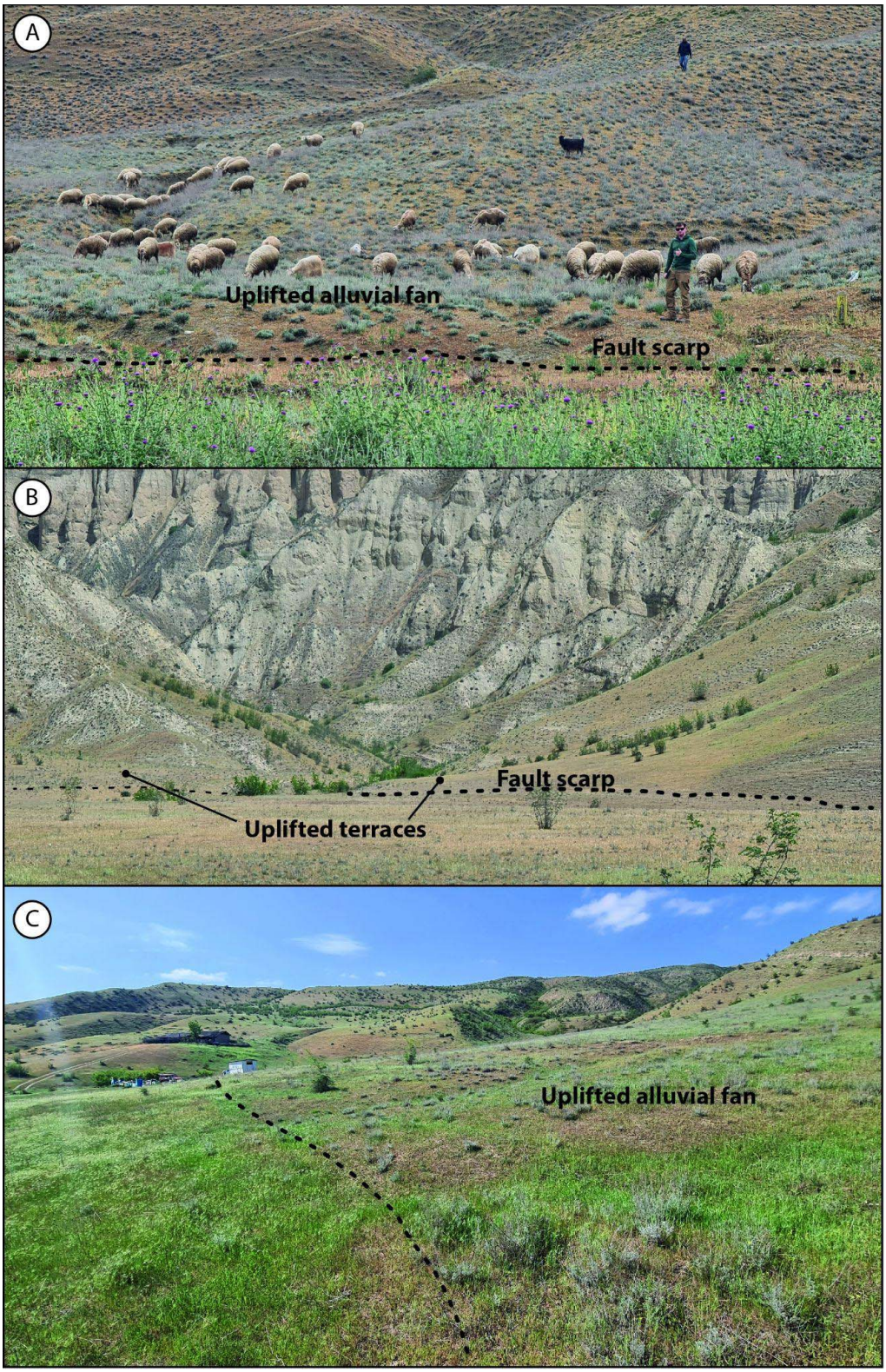

Figure 2. Fault scarps in young geomorphic surfaces show that each of the major thrusts in the Kura fold-thrust belt is active. Locations indicated on Figure 1.

3 Results

3.1 Fault Mapping

Our field reconnaissance focused on the easternmost 60 km of the Kura fold-thrust belt from near Goychay to Agsu (**Figure 1**). This section of the thrust-belt consists of two major thrust sheets that each comprise several imbricate thrusts. The more northerly sheet forms the Längäiz ridge, which is a relay ramp that steps near Goychay. The southerly sheet begins to the east of Goychay and increases in relief eastward as it forms a large anticline (the Garamäyäm ridge) before tapering and finally disappearing just south of Agsu. Near the center of the Garamäyäm ridge the southerly sheet is split into two thrusts, which merge eastward. Field surveys revealed fault scarps and uplifted youthful geomorphic surfaces on all of these different fault strands (**Figure 2**), which suggests that each of these thrusts has been active in the Holocene and periodically ruptures to the ground surface during large earthquakes.

3.2 Paleoseismic Trenching

3.2.1 Description of Trench Site

The Kura thrust immediately adjacent to Agsu follows the rangefront of the Greater Caucasus. Here the active fault forms a ~50-m-high back-tilted uplifted bench along the rangefront, with a clear fold in the crest of the uplifted surface (**Figure 3**). Approximately 2.5 km east of Agsu is a small alluvial valley where a stream has incised through this bench, cutting perpendicularly to the fault trace (**Figures 3 and 4**). This valley contains two low incised terraces, a lower T1 terrace and a 1-m-higher T2 terrace. The two terrace treads are smooth, relatively flat, and continuously traceable upstream from the valley mouth for ~300 m (**Figure 4A**). At the valley mouth, both terraces are displaced, with fault scarps that are ~2 m high. On the western margin of the valley a small stream has sharply incised into the T1 terrace. The drone-derived hillshade image shows evidence of anthropogenic modification of the scarp in the T2 terrace, but both sides of the fault in the T1 terrace appear to be unmodified and correlative. A paleoseismic trench was excavated across the 2-m-high scarp cutting across the T1 terrace in this alluvial valley.

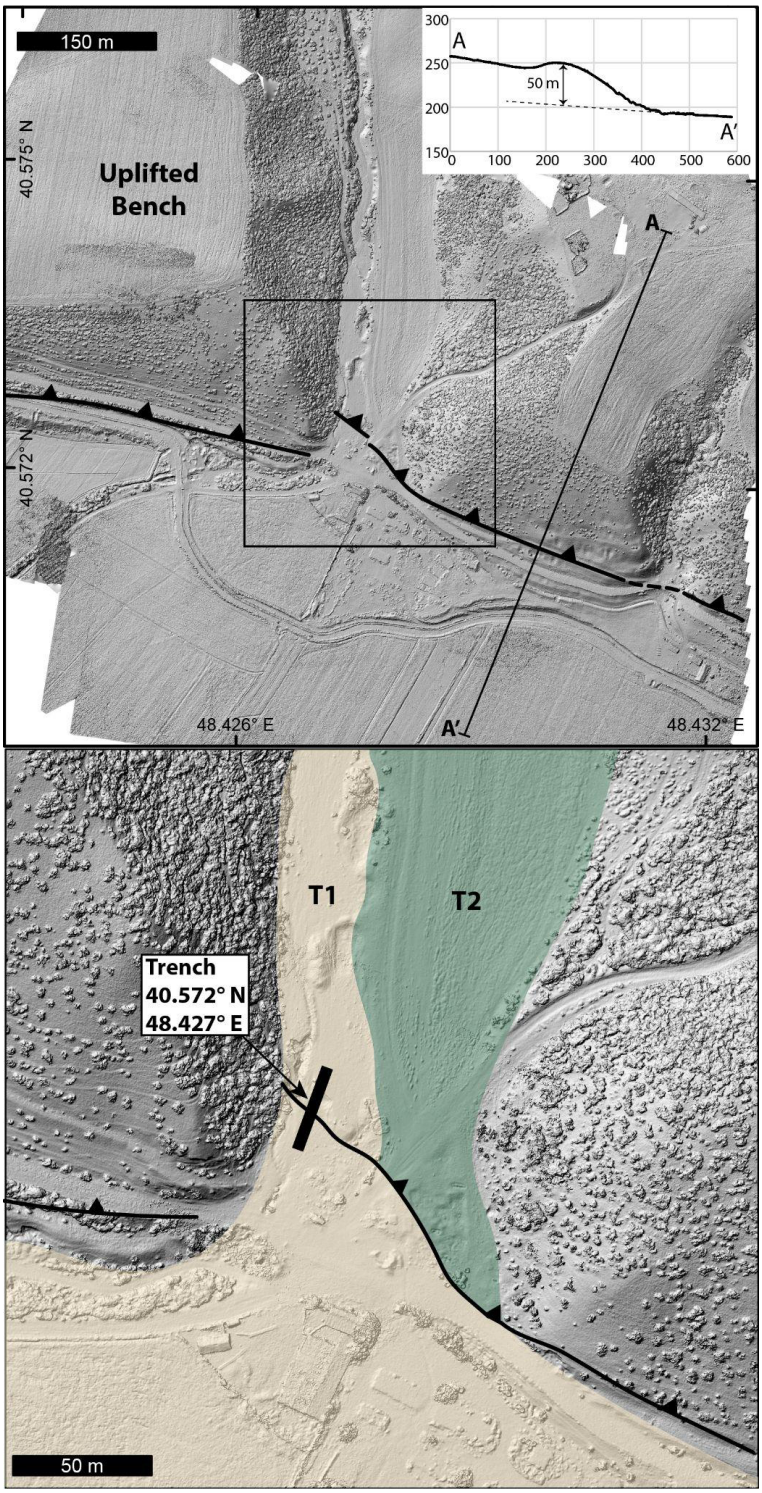

Figure 3. Hillshade image of photogrammetry-derived DEM of the trench site east of Agsu. Inset topographic profile shows characteristic folding of the 50-m-high uplifted bench along the rangefront here. Lower panel shows T1 and T2 terraces within the small alluvial valley.

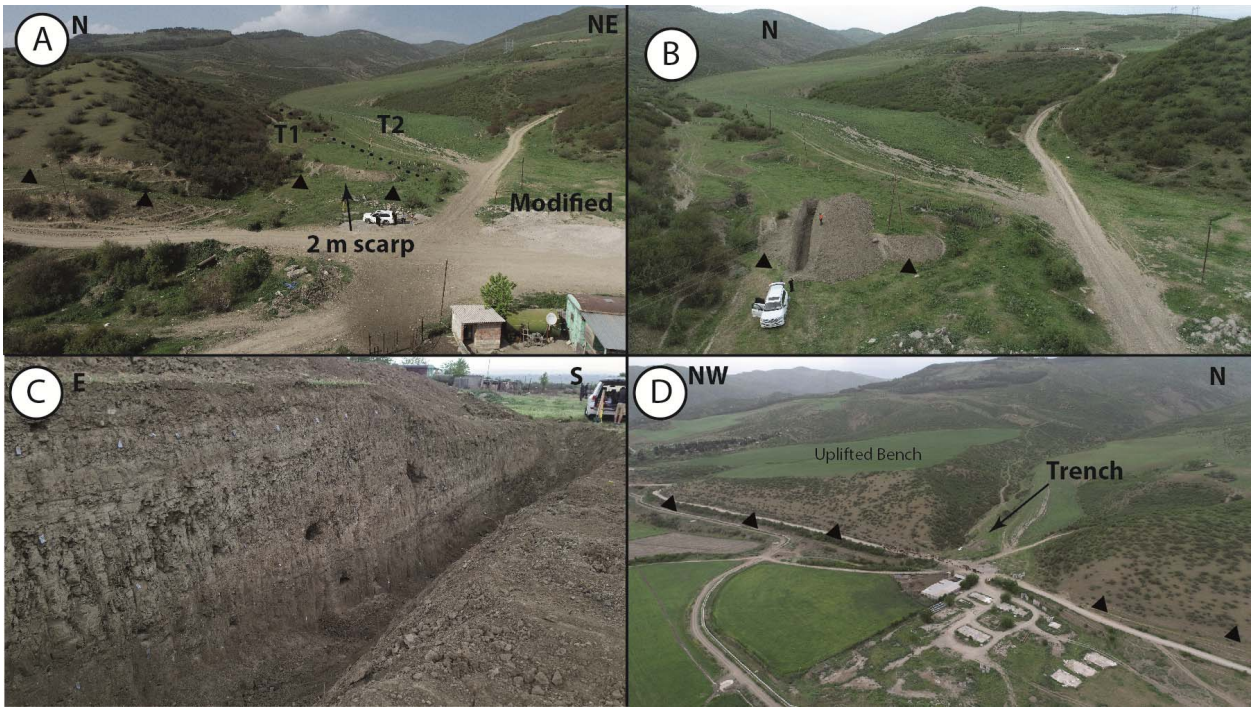

Figure 4. Aerial photographs of the trench site before (A) and after (B) trench excavation, highlighting the 2-m-high scarp and small alluvial valley. (C) shows the excavated trench. (D) shows the uplifted folded bench along the rangefront.

3.2.2 Description of Trench Exposure

The trench exposure was 22-m-long and 5-m-deep (**Figure 5**). The trench revealed a series of clays, alluvium, and colluvium that are cut and deformed by a low angle fault. The lowest unit in the trench, U1, is a colluvial deposit that consists of poorly sorted rounded cobbles and gravels in a fine grained silty/sandy matrix. Onlapping onto U1 is U2, a south-thickening sequence of interbedded, well-sorted, grain-supported fluvial sands, gravels, and rounded cobbles. At the top of U2 is a ~40-cm-thick fine grained, light colored paleosol, that is readily traced across much of the trench. Above U1 in the hanging wall is U3, a 1.5-m-thick finely laminated clay that dries into prismatic blocks, and is highly sheared near the fault zone. Above U3 is U4, a sequence of clays, silts and sands with fine laminations. Above U4 is U5, a series of laminated silts and sands with a thin layer of cobbles, and scattered modern plastic garbage in the upper 20-30 cm. Above U2 is a poorly sorted colluvial unit, W1, composed of rounded cobbles and gravels in a fine grained matrix. At the top of W1 is a ~20-cm-thick, light-colored fine-grained paleosol. W1 is thickest directly below the fault scarp and tapers away from the scarp to the south. Above W1 is W2. W2 is another colluvial unit, composed of angular blocks of clay in a fine grained matrix with very few scattered pebbles.

A sub-horizontal fault cuts across the trench exposure and splays into 4 sub-faults in the hanging wall (faults F1 to F4). Fault F4 forms a shear zone within U3. Faults F3 and F2 bound a shear zone composed of materials from U1 and are well marked by alignments of cobbles and pebbles. Fault F1 displaces part of the soil capping U2. Units U1, U2, U3, and U4 are clearly folded in the hanging wall of the trench, while U2 is largely undeformed in the footwall.

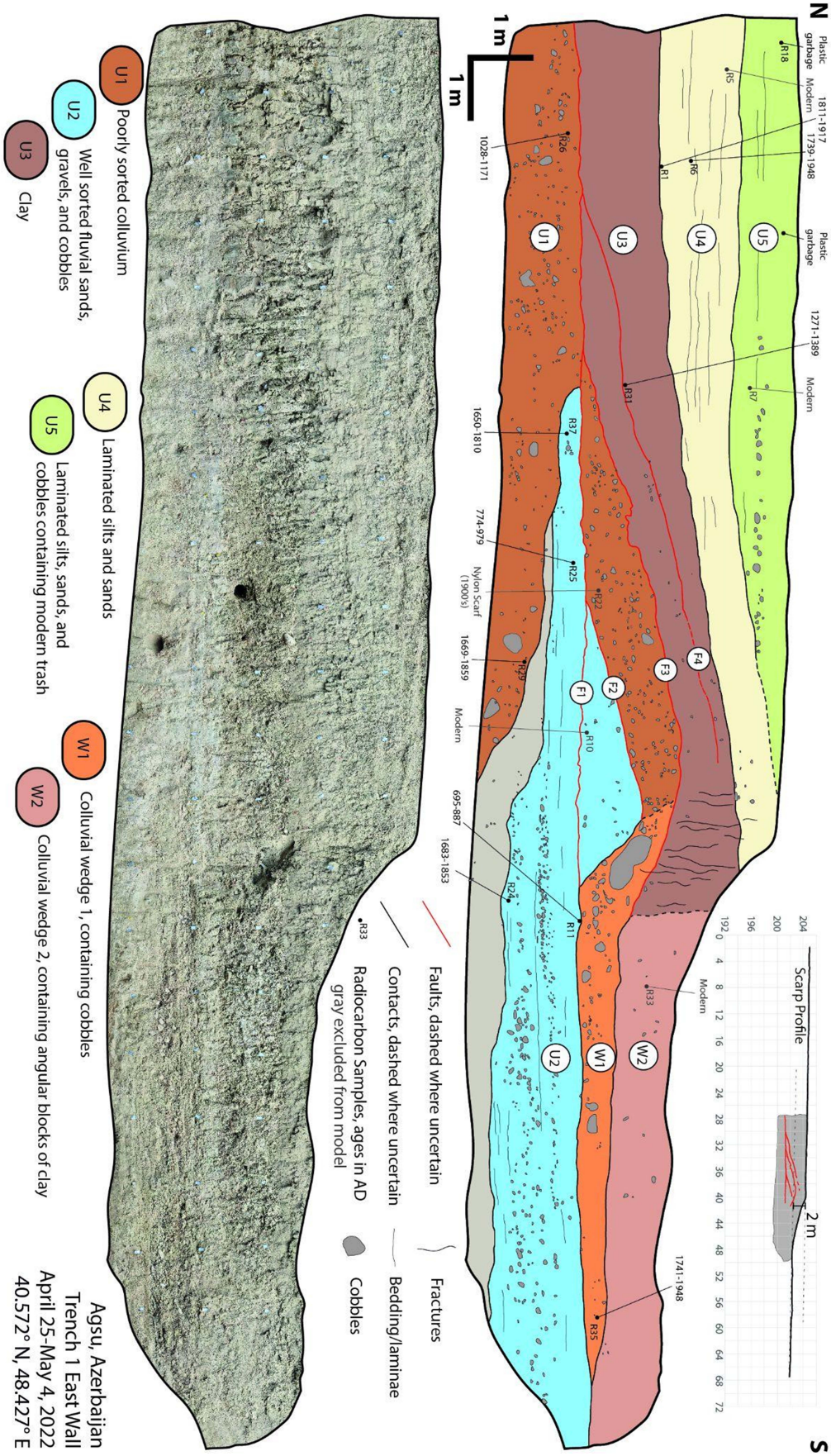
N
S
1 m
1 m
Plastic garbage
Modern
1811-1917
1739-1948
Plastic garbage
1271-1389
Modern
1650-1810
774-979
Nylon Scarf (1900's)
1669-1859
Modern
695-887
1683-1853
1028-1171
1741-1948
R18
R5
R1
R6
R26
R31
R7
R37
R25
R22
R23
R10
R24
R11
R33
R35
U1
U2
U3
U4
U5
F1
F2
F3
F4
W1
W2
Scarp Profile
2 m
204
200
196
192
0
4
8
12
16
20
24
28
32
36
40
44
48
52
56
60
64
68
72
Modern
U1 Poorly sorted colluvium
U2 Well sorted fluvial sands, gravels, and cobbles
U3 Clay
U4 Laminated silts and sands
U5 Laminated silts, sands, and cobbles containing modern trash
W1 Colluvial wedge 1, containing cobbles
W2 Colluvial wedge 2, containing angular blocks of clay
Faults, dashed where uncertain
Contacts, dashed where uncertain
R33 Radiocarbon Samples, ages in AD gray excluded from model
Fractures
Bedding/laminae
Cobbles
Agsu, Azerbaijan
Trench 1 East Wall
April 25-May 4, 2022
40.572° N, 48.427° E

Figure 5 (previous). Trench log (upper) and photomosaic (lower) of the east wall of the Agsu trench. Inset shows position of trench within fault scarp profile. Ages listed are modeled ages as described in text. We interpret evidence of two events primarily based on the colluvial wedge stratigraphy on the footwall (W1 and W2).

3.2.3 Event History

The stratigraphy on the southern half of the trench provides evidence of two rupturing events, clearly demarcated by the two distinct colluvial wedges (W1 & W2) resting upon undeformed fluvial sediments (U2) (**Figure 5**). The older, penultimate event (E1) produced the W1 colluvial wedge composed of unsorted gravels and cobbles that bury the paleosol capping the lower U2 fluvial sediments. This W1 wedge then developed a thin, fine-grained soil on its top. The younger, most recent event (E2) produced another colluvial wedge (W2), but composed of angular blocks of clay sourced from U3. This W2 wedge buried the thin soil capping the W1 penultimate wedge.

The penultimate E1 event ruptured the F1 and F2 faults through the U1 colluvial deposit at the bottom of the north-half of the trench along a sub-horizontal fault plane. This created an abrupt fold in this U1 colluvial deposit, which then collapsed forming the E1 wedge. The clays and silts of U4 were then deposited on the hanging wall, behind this fold. A minimum of 6.6 m of displacement can be estimated for E1 by backslipping U1 along faults F1 and F2.

The more recent event, E2, ruptured the F3 fault along the base of the U3 clay, folding units U3 and U4 into a sharp fold-scarp, and again creating a colluvial wedge, W2. U5, like U4, represents growth strata deposited behind this fold on the hanging wall. A minimum of 3.5 m of displacement is required to thrust U3 over the crest of the fold in U1. As units U1 and U3 are both highly sheared in the fault zone, there is high uncertainty in these offset measurements.

3.2.4 ^{14}C Geochronology

The radiocarbon ages of 14 total samples of charcoal, organic sediments, and plant fragments recovered from the strata were measured by Beta Analytic laboratories in Miami, Florida. The sample locations are indicated on **Figure 5**, and the results are listed in **Table 1**. Four samples: R5, R7, R10, and R33 yielded modern ages. Of these, R7 and R33 are from post-earthquake deposits, so the modern ages may be representative of their depositional ages, but due to uncertainty in the calibration of modern radiocarbon we exclude them from our OxCal model. R5 and R10, from within layers dated to pre-modern by other samples, are both plant materials so it is likely that we inadvertently sampled modern plant roots, and thus we exclude them from further analysis. Sample R22, from within the fault zone (Unit U1), is a large fragment of a nylon scarf. Nylon was invented in the mid 1900's so we think that this material must have been brought down to this level by a burrowing animal, as other samples from Unit 1 are medieval in age (R26: 1028-1171, R29: 1669-1859). Sample R18 was a late 1990's vintage plastic candy wrapper, so is assumed to be from AD 1995 ± 5, and is used as an upper limit of the stratigraphic model. The remaining ages were placed into a sequence model and calibrated using OxCal v4.4 (Bronk Ramsey, 1995) (**Figure 6**). The result of this model places limits on the timing of the two surface rupturing events: E1 occurred from AD 1713-1895, and E2 occurred from AD 1872-2003 (95.4% confidence intervals).

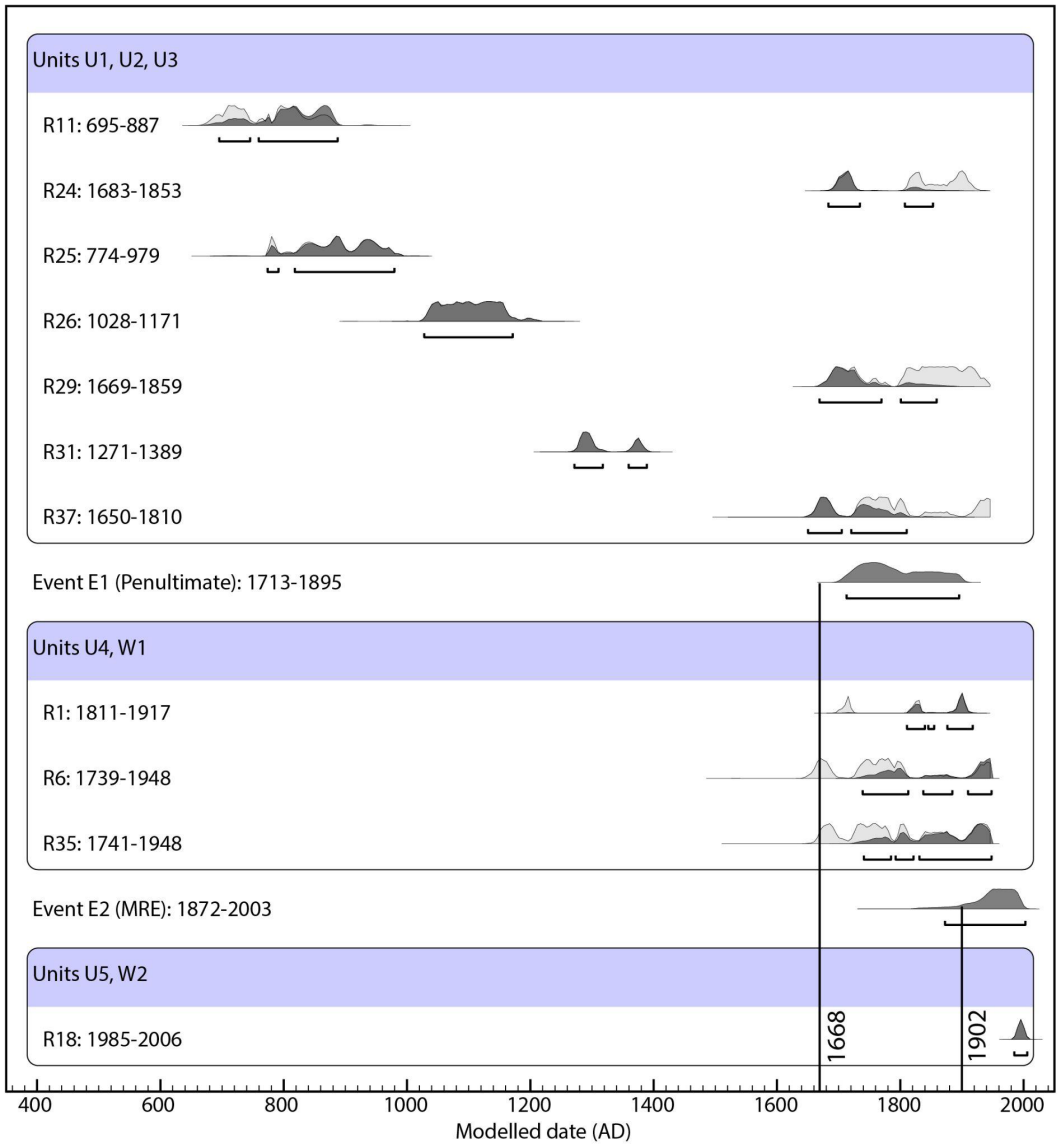

Figure 6. OxCal model of radiocarbon samples and event ages. The timing of the 1668 and 1902 historical earthquakes are plotted for reference. Event horizons for E1 and E2 are AD 1713-1895 and AD 1872-2003, respectively.

3.3 Slip Rate Measurement

West of Agsu in the foreland is the Garamäyän ridge, a prominent pair of west-northwest-striking active folds are cut by a series of water gaps (Forte et al., 2013). In one of these water gaps ("Gap 2" of Forte et al., 2013) is an inset strath terrace that sits ~20 m above the modern stream. The southern margin of this terrace is abruptly truncated by an active fault and shows a sharp anticline close to the head of the fault scarp. In a cliff exposure cut for an irrigation canal we found a strath of subhorizontal fluvial cobbles capping sub-vertical sand and gravel beds **(Figure 7**). The radiocarbon age dating of a single gastropod shell (WG1, **Table 1**) sampled from within these horizontal sediments allows for calculation of a vertical uplift rate for this fault (Pigati et al., 2010). The OxCal calibrated age of the shell is 6975-6791 cal BP. As shells can contain significant inherited carbon, this should be considered to be the oldest possible

age of the deposit. Dividing the 20 m uplift of the terrace (**Figure 7B**) by this age results in an average vertical uplift rate of 2.9 mm/yr.

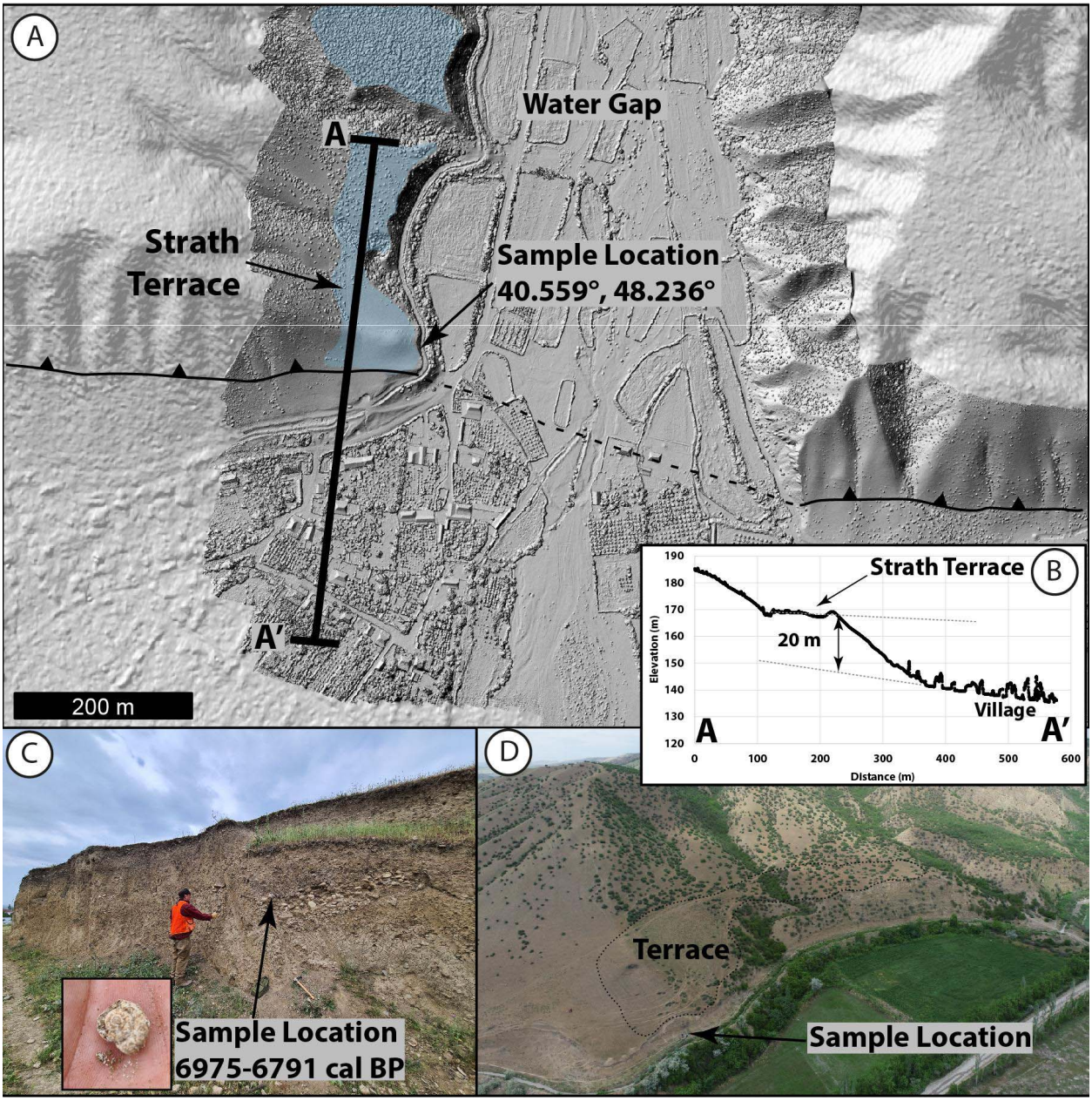

Figure 7. Hillshade image of photogrammetry-derived DEM (A) showing the uplifted strath terrace inset to the watergap. Profile A-A' shown in (B) shows 20 m of uplift. A gastropod shell (inset) was sampled from subhorizontal fluvial cobbles in an exposure of the strath (C). Oblique aerial photograph of the terrace (D).

4 Discussion

4.1 Distribution of Slip in the foreland of the Greater Caucasus

Converting our 2.9 mm/yr uplift rate at the water gap site (**Figure 7**) to dip-slip and shortening- rates requires an assumption of subsurface structural geometry. Forte et al. (2013) model the Garamäyän ridge anticline as a blind fault-propagation fold controlled by a 20° northeast dipping thrust fault that has accommodated 5.6 km of shortening. Our field investigations revealed the presence of surficial fault scarps demonstrating that this fault is not blind. If we assume this 20° dipping thrust fault geometry, and that folding is minimal over the relatively short ~7 kyr timescale, then 2.9 mm/yr of uplift corresponds to 8.0 mm/yr of shortening and a dip-slip rate of 8.5 mm/yr. These rates are in-line with the prior structural and geodetic estimates across the Kura fold-thrust belt (Forte et al., 2013; Kadirov et al., 2012). Unfortunately, due to the reliance of our calculations on a single age and the uncertainty of the near-surface fault geometry, the uncertainty of our rates is difficult to quantify. However, as this rate was determined from only one of the two main active parallel structures at this longitude (the other was trenched in this study), and this rate consumes nearly all of the budget of the prior estimates, we expect that this rate is an upper limit. Regardless, this result is consistent with that of Forte et al. (2013), which demonstrates that a significant portion (~80-100%) of both the post-1.5 Ma and present-day geodetic strain budget across the Greater Caucasus is accommodated by the Kura thrust belt.

4.2 Historical Earthquakes

While the Eastern Caucasus have not experienced any M>7 earthquakes during the instrumental period (Telesca et al., 2018; Yetirmishli et al., 2021), the region has experienced numerous pre-instrumental devastating earthquakes, the largest (M~7) occurring in AD 1139, 1668, and 1902 (Ismail-Zadeh, 2020). The widely felt 1668 and 1902 earthquakes both destroyed the medieval capital city of Shamakhi (**Figure 1**), while moderate (M~6) events in 1828, 1859, 1869, and 1872 caused severe damage to the city.

The 1139 earthquake is reported to have destroyed the city of Ganja in the southwestern part of the Kura basin (**Figure 1a**). It is unclear whether this event is associated with the Kura fold-thrust belt, or if it occurred in the Lesser Caucasus. However, the AD 1139 earthquake is the earliest earthquake record from the Kura region, and as the region has been continuously inhabited since then, we assume that all significant large earthquakes since that time have been reported.

A fair amount of detail can be gleaned about the 1668 Shamakhi earthquake from contemporary historical sources (reported dates range from 1667-1669). Some of the most widely cited accounts of the damage in Western studies come from European travelers passing through the region around this period. The well-known French traveler, John Tavernier, was in the region during the earthquake but only heard news of the event while in Tabriz. According to the account he received the entire city was demolished and only a handful of people survived (Tavernier, 1678). Somewhat later, Cornelius de Bruijn (translated into English as “Cornelius le Brun") visited Shamakhi, and mentioned that the earthquake, which occurred thirty-five years before his travels in 1703, destroyed all of the city walls and major monuments including the congregational mosque (Le Brun, 1759). It would appear, however, that the administrative

function of the city remained and he mentions smaller mosques and houses that he saw when visiting. The impact on the people was severe enough that a tremor during his visit (1703) saw people flee the city but there was limited or no damage to structures. It is worth noting that de Bruijn's dating places this event in 1668, a date accepted by Nikonov in his comprehensive review of the source materials for this earthquake, more specifically he estimates, on the 14th January (Nikonov, 1982). In his chronological table of events, he notes a number of aftershocks ranging from later in 1668, until early 1671. Specific impacts listed by Nikonov based on his assessment of all sources available to him include: destruction of the entire city, between 6,000-8,000 deceased, large numbers of collapsed individual buildings including the city walls and fortress, and landslides causing loss of life (Nikonov, 1982). Sources collated in this work detailing other settlements in the region mention impacts as far away as Baku (a collapsed wall of a palace), detection but no damage in Derbent, and the event was apparently not felt in the more distant heavily-populated regions of Tbilisi or Yerevan. Based on the collective data, Nikonov assesses the area of highest impact of the earthquake as IX on the MSK-64 intensity scale in the region of Shamakhi.

The 1828 event destroyed 526 buildings across the region. The 1859 event killed 100 people, and destroyed 741 buildings, prompting the capital to be relocated from Shamakhi to Baku. The 1872 event killed 118 people and destroyed all but 20 buildings (Shebalin et al., 1982). The 1902 event killed 2,000 people and destroyed 4,000 homes (New York Times, 1902). An isoseismal plot of damaged buildings from the 1902 earthquake (adapted from Weber, 1903 in **Figure 1**) suggests that the epicenter was close to Shamakhi and that the fault that ruptured follows the overall strike of the Kura thrust.

Our paleoseismic results provide evidence of two surface rupturing events since the early 18th century (E1: AD 1713-1895 and E2: AD 1872-2003). The younger of these rupturing events, E2, may be the surface rupture of the 1902 Shamakhi earthquake, while the penultimate E1 event could be the 1668 earthquake if we reject two radiocarbon ages (R24 and R29). Present-day Shamakhi is only ~18 km northeast of the Agsu trench site, and would have experienced high intensity ground motions if the northeast-dipping fault ruptured, so the destruction reported during these events is consistent with our paleoseismic results.

The past magnitude estimate of M~7 for the 1902 E2 event is reasonable based on comparisons of the 3.5 m displacement in the trench to displacements of other surface rupturing reverse mechanism earthquakes (e.g. Wesnousky, 2008), though such comparisons are of limited utility due to the paucity of examples of thrust/reverse surface rupturing earthquakes. Based on the greater observed displacement, E1 may have had a larger magnitude than E2. If we assume that the 1902 rupture plane (E2) has dimensions similar to the reported high damage isoseismals (50 x 30 km, Weber, 1903) and slipped an average of 3.5 m (measured from the trench), then using the equation relating moment magnitude to seismogenic moment, where l=rupture length (50 km), w=rupture width (30 km), and d=displacement (3.5 m) (Hanks and Kanamori, 1979, adapted for dyne-cm):

$$Mw = \frac{2}{3} log(3 \times 10^{11} \times l \times w \times d \times 10^{12} + 1) - 10.73$$

The result is an estimated M_w 7.4, much higher than the past estimate of M6.9 from intensity data for the 1902 Shamakhi earthquake.

The lack of reported historical earthquakes farther to the west in the Kura fold-thrust belt (i.e., near Goychay and west) contrasts with the numerous earthquakes reported near Shamakhi over the past 4 centuries. Like prior authors, we expect that most large (e.g. Mw>7) earthquakes

would have been felt over a wide area and likely would have been recorded (Jackson and Ambraseys, 1997). Thus, the western and central Kura fold-thrust belt could either (a) have considerable strain accumulated or (b) be deforming aseismically. Given the numerous fault scarps identified during fieldwork (**Figure 2**) we suggest that the fault system does periodically produce surface rupturing earthquakes. If we assume that strain has accumulated at a rate of ~10 mm/yr since the earliest reported earthquake in AD 1139, then it is possible that 250 km of the Kura fold-thrust belt, from Agsu to Tbilisi, could have >8.8 m of stored strain. The Kura fold-thrust belt soles into a 5° north-dipping detachment at a depth of ~5 km (Forte et al., 2013), and the minimum width of the thrust belt is ~25 km. The base of the seismogenic zone extends to at least a depth of 40 km in this region (Gunnels et al., 2021; Yetirmishli et al., 2021). Based on this geometry (width, w=25 km, length, l=250 km, displacement, d=8.8), we can estimate a magnitude, were the whole fault to rupture, using the above equation. The result demonstrates that the Kura fold-thrust belt could have sufficient stored strain to produce a Mw>8 earthquake. This represents a significant hazard to the populations and infrastructure of the region, including the large earthen dam and 15,730 km^3 reservoir at Mingecevir (**Figure 1**).

This contrast in earthquake histories between the main Kura fold-thrust belt and the eastern region near Shamakhi suggests that ruptures to the west are less frequent but could be significantly larger, while the Shamakhi region is affected by more frequent moderate ruptures. More paleoseismic trenching and detailed mapping will be required to confirm our results, ascertain the size of past ruptures in the Kura fold-thrust belt and to investigate how these ruptures are partitioned among the different thrust sheets.

5 Conclusions

The two surface rupturing events (AD 1713-1895 and AD 1872-2003) from the trench near Agsu are likely the surface ruptures of the historical 1668 and 1902 earthquakes that destroyed Shamakhi. We reassess the estimated magnitude for the 1902 event and suggest that it was a Mw7.4 rather than M6.9 earthquake. Further trenching is required to confirm these results, to place limits on the possible rupture lengths, to better estimate the magnitude of these historical events, and to determine the rupture histories of the other faults in the Kura fold-thrust belt to the west. Dating of an abandoned strath terrace in a water gap provides a maximum limit of ~8 mm/yr of shortening during the Holocene across the youngest active folds west of Agsu. These results are consistent with geodetic and structural studies that show that most of the ~10 mm/yr of convergence between the Arabian plate and Eurasia in the western Greater Caucasus is accommodated by the Kura fold-thrust belt. Based on these rates, and if there have been no ruptures of the central and western parts of the Kura fold-thrust system since the last reported historical event in 1139 AD, then the system could have sufficient strain accumulated to produce a M>8 earthquake.

Acknowledgements

This research was supported in part by the Leverhulme Trust projects ‘EROICA’ (RPG-2018-371) and ‘NEPTUNE’ (RPG-2018-243), by the NERC-ESRC Increasing Resilience to Natural Hazards program ‘Earthquakes without Frontiers’ (NE/J02001X/1), the NERC-funded COMET (GA/13/M/031) and allocation 0009090 from the Research England GCRF support fund. The authors are grateful for field assistance from Sarvat Gurbanzada, Rashid Khalilov, Aslan Sadikov, Telman Jaferov, and Samandar Mammadov. Thanks to Arzu Javadova (SOCAR)

and Nazim Abdullayev (BP) for both their scientific input and for helping to organize funding from BP for field and laboratory expenses.

Data Availability Statement

Drone photogrammetry models produced during this study are freely available on OpenTopography.org: https://doi.org/10.5069/G93776XH
All other data used is publicly available or provided in this manuscript.

Conflict of Interest Statement

The authors have no relevant financial or non-financial interests to disclose.

References

Avdeev, B., Niemi, N.A., 2011. Rapid Pliocene exhumation of the central Greater Caucasus constrained by low-temperature thermochronometry. Tectonics 30. https://doi.org/10.1029/2010TC002808

Bronk Ramsey, C., 1995. Radiocarbon Calibration and Analysis of Stratigraphy: The OxCal Program. Radiocarbon 37, 425–430. https://doi.org/10.1017/S0033822200030903

Cowgill, E., Forte, A.M., Niemi, N., Avdeev, B., Tye, A., Trexler, C., Javakhishvili, Z., Elashvili, M., Godoladze, T., 2016. Relict basin closure and crustal shortening budgets during continental collision: An example from Caucasus sediment provenance. Tectonics 35, 2918–2947. https://doi.org/10.1002/2016TC004295

Forte, A.M., Cowgill, E., Murtuzayev, I., Kangarli, T., Stoica, M., 2013. Structural geometries and magnitude of shortening in the eastern Kura fold-thrust belt, Azerbaijan: Implications for the development of the Greater Caucasus Mountains. Tectonics 32, 688–717. https://doi.org/10.1002/tect.20032

Forte, A.M., Sumner, D.Y., Cowgill, E., Stoica, M., Murtuzayev, I., Kangarli, T., Elashvili, M., Godoladze, T., Javakhishvili, Z., 2015. Late Miocene to Pliocene stratigraphy of the Kura Basin, a subbasin of the South Caspian Basin: implications for the diachroneity of stage boundaries. Basin Res. 27, 247–271. https://doi.org/10.1111/bre.12069

Gunnels, M., Yetrimishli, G., Kazimova, S., Sandvol, E., 2021. Seismotectonic evidence for subduction beneath the Eastern Greater Caucasus. Geophys. J. Int. 224, 1825–1834. https://doi.org/10.1093/gji/ggaa522

Hanks, T.C., Kanamori, H., 1979. A moment magnitude scale. J. Geophys. Res. Solid Earth 84, 2348–2350. https://doi.org/10.1029/JB084iB05p02348

Ismail-Zadeh, A., Adamia, S., Chabukiani, A., Chelidze, T., Cloetingh, S., Floyd, M., Gorshkov, A., Gvishiani, A., Ismail-Zadeh, T., Kaban, M.K., Kadirov, F., Karapetyan, J., Kangarli, T., Kiria, J., Koulakov, I., Mosar, J., Mumladze, T., Müller, B., Sadradze, N., Safarov, R., Schilling, F., Soloviev, A., 2020. Geodynamics, seismicity, and seismic hazards of the Caucasus. Earth-Sci. Rev. 207, 103222. https://doi.org/10.1016/j.earscirev.2020.103222

Jackson, J., Priestley, K., Allen, M., Berberian, M., 2002. Active tectonics of the South Caspian Basin. Geophys. J. Int. 148, 214–245. https://doi.org/10.1046/j.1365-246X.2002.01588.x

Jackson, J.A., Ambraseys, N.N., 1997. Convergence between Eurasia and Arabia in eastern Turkey and the Caucasus, in: Historical and Prehistorical Earthquakes in the Caucasus, 28. pp. 79–90.

Kadirov, F., Floyd, M., Alizadeh, A., Guliev, I., Reilinger, R., Kuleli, S., King, R., Nafi Toksoz, M., 2012. Kinematics of the eastern Caucasus near Baku, Azerbaijan. Nat. Hazards 63, 997–1006. https://doi.org/10.1007/s11069-012-0199-0

Kangarli, T.N., Kadirov, F.A., Etirmishli, G.D., Aliev, F.A., Kazimova, S.E., Aliev, A.M., Safarov, R.T., Vakhabov, U.G., 2018. Geodynamics, active faults and earthquake source mechanisms in the zone of pseudosubduction interaction of continental microplates in the South and North Caucasus (southern slope of the Greater Caucasus, Azerbaijan). Geodyn. Tectonophys. 9, 1099–1126. https://doi.org/10.5800/GT-2018-9-4-0385

Le Brun, C., 1759. A New and More Correct Translation than Has Hitherto Appeared in Public of Mr. Cornelius Le Brun's Travels into Moscovy, Persia, and Divers Parts of the East-Indies; Containing An Accurate Description of All Such Articles as Are Most Remarkable in Each of Those Different Countries, and Most Worthy the Attention of the Curious Reader. As Also Of Their Antiquities; but More Particularly Those Relating to the Famous Palace of Persepolis, Commonly Called Chelminar by the Persians: By a Gentleman of Oxford. J. Warcus, London.

McCalpin, J. (Ed.), 2009. Paleoseismology, 2nd ed. ed, International geophysics series. Academic Press, Burlington, MA.

McKenzie, D., 1972. Active Tectonics of the Mediterranean Region. Geophys. J. Int. 30, 109–185. https://doi.org/10.1111/j.1365-246X.1972.tb02351.x

Mosar, J., Kangarli, T., Bochud, M., Glasmacher, U.A., Rast, A., Brunet, M.-F., Sosson, M., 2010. Cenozoic-Recent tectonics and uplift in the Greater Caucasus: a perspective from Azerbaijan. Geol. Soc. Lond. Spec. Publ. 340, 261–280. https://doi.org/10.1144/SP340.12

Mumladze, T., Forte, A.M., Cowgill, E.S., Trexler, C.C., Niemi, N.A., Burak Yıkılmaz, M., Kellogg, L.H., 2015. Subducted, detached, and torn slabs beneath the Greater Caucasus. GeoResJ 5, 36–46. https://doi.org/10.1016/j.grj.2014.09.004

New York Times, T., 1902. 2,000 DEAD AT SHEMAKHA. N. Y. Times 1.

Nikonov, A.A., 1982. Sil'neĭshee Zemletriasenie Bol'shogo Kavkaza 14 Ianvaria 1668 g. Fis. Zemli 9, 90–106.

Philip, H., Cisternas, A., Gvishiani, A., Gorshkov, A., 1989. The Caucasus: an actual example of the initial stages of continental collision. Tectonophysics 161, 1–21. https://doi.org/10.1016/0040-1951(89)90297-7

Pigati, J.S., Rech, J.A., Nekola, J.C., 2010. Radiocarbon dating of small terrestrial gastropod shells in North America. Quat. Geochronol. 5, 519–532. https://doi.org/10.1016/j.quageo.2010.01.001

Reilinger, R., McClusky, S., Vernant, P., Lawrence, S., Ergintav, S., Cakmak, R., Ozener, H., Kadirov, F., Guliev, I., Stepanyan, R., Nadariya, M., Hahubia, G., Mahmoud, S., Sakr, K., ArRajehi, A., Paradissis, D., Al-Aydrus, A., Prilepin, M., Guseva, T., Evren, E., Dmitrotsa,

A., Filikov, S.V., Gomez, F., Al-Ghazzi, R., Karam, G., 2006. GPS constraints on continental deformation in the Africa-Arabia-Eurasia continental collision zone and implications for the dynamics of plate interactions. J. Geophys. Res. Solid Earth 111. https://doi.org/10.1029/2005JB004051

Shebalin, N.V., Kondorskaia, N.V., World Data Center A for Solid Earth Geophysics, 1982. New catalog of strong earthquakes in the U.S.S.R. from ancient times through 1977, Report SE ;31. World Data Center A for Solid Earth Geophysics, Boulder, Colo.

Tavernier, J.-B., 1678. The Six Voyages of John Baptista Tavernier, a Noble Man of France Now Living, through Turky into Persia and the East-Indies, Finished in the Year 1670 : Giving an Account of the State of Those Countries : Illustrated with Divers Sculptures ; Together with a New Relation of the Present Grand Seignor's Seraglio, by the Same Author. John Philips, London.

Telesca, L., Kadirov, F., Yetirmishli, G., Safarov, R., Kazimova, S., 2018. Joint Use of Seismological and Topological Statistical Methods for the Analysis of 2010–2016 Azerbaijan Seismicity. Pure Appl. Geophys. 175, 4225–4239. https://doi.org/10.1007/s00024-018-1945-3

Weber, V., 1903. Shamakhi Earthquake of 13 February 1902, Proceedings of the St. Petersburg Geological Committee.

Yetirmishli, G.J., Ismayilova, S.S., Kazimova, S.E., 2021. Seismicity of the territory of Azerbaijan in 2019. Seism. Obs. Territ. Azerbaijan 19, 3–18.

Yetirmishli, G.J., Kazimov, I.E., Kazimova, A.F., 2022. Analysis of Modern Movements of Earth Crust Blocks in Azerbaijan According to the Data of GPS Stations in 2020-2021. Seism. Obs. Territ. Azerbaijan 21, 19–24.

Zhang, H., Aldana-Jague, E., Clapuyt, F., Wilken, F., Vanacker, V., Van Oost, K., 2019. Evaluating the potential of post-processing kinematic (PPK) georeferencing for UAV-based structure- from-motion (SfM) photogrammetry and surface change detection. Earth Surf. Dyn. 7, 807–827. https://doi.org/10.5194/esurf-7-807-2019

488 **Table 1. Radiocarbon sample data**

Sample Name	Location	Unit	Lat. (°)	Lon. (°)	Sample Material[1]	Radiocarbon Age (BP)	Calibrated[2] Age (AD)	OxCal[2] v4.4 Modeled Age (AD, 95.4%)	Percent Modern Carbon (pMC)	δ13C (‰)	δ18O (‰)
R1	Agsu T1	U4	40.572	48.427	Charcoal	-20 ± 30	1954-1957 (60.9%) 1886-1913 (31.0%) 1707-1718 (2.4%) 1825-1832 (1.2%)	1811-1917	100.25 ± 0.37	-27.0	-
R5	Agsu T1	U4	40.572	48.427	Plant material	-2080 ± 30	1978-1979 (89.3%) 1961 (6.1%)	-	129.55 ± 0.48	-24.8	-
R6	Agsu T1	U4	40.572	48.427	Charcoal	190 ± 30	1724-1812 (52.0%) 1648-1695 (21.8%) 1916- >1950(17.8%) 1838-1878 (3.8%)	1739-1948	97.66 ± 0.36	-24.9	-
R7	Agsu T1	U5	40.572	48.427	Plant material	-770 ± 30	1996-2000 (92.9%) 1956-1957 (2.5%)	-	110.06 ± 0.41	-28.0	-
R10	Agsu T1	U2	40.572	48.427	Plant Material	-3410 ± 30	1967-1971 (93.2%) 1962 (2.2%)	-	152.88 ± 0.57	-25.8	-
R11	Agsu T1	U2	40.572	48.427	Plant Material	1240 ± 30	758-880 (55.8%) 679-746 (39.6%)	695-887	85.7 ± 0.32	-26.3	-
R18	Agsu T1	U5	40.572	48.427	Plastic candy wrapper	-	-	1985-2006	-	-	-
R24	Agsu T1	U2	40.572	48.427	Charcoal	70 ± 30	1810-1919 (68.7%) 1692-1727 (26.7%)	1683-1853	99.13 ± 0.37	-23.5	-
R25	Agsu T1	U2	40.572	48.427	Organic Sediment*	1160 ± 30	820-978 (83.9%) 772-790 (10.2%) 804-810 (1.3%)	774-979	86.55 ± 0.32	-	-
R26	Agsu T1	U1	40.572	48.427	Organic Sediment*	940 ± 30	1028-1172 (95.4%)	1028-1171	88.96 ± 0.33	-26.2	-
R29	Agsu T1	U1	40.572	48.427	Charcoal	120 ± 30	1799-1940 (67.2%) 1680-1740 (25.8%) 1752-1764 (2.4%)	1669-1859	98.52 ± 0.37	-26.3	-
R31	Agsu T1	U3	40.572	48.427	Charcoal	690 ± 30	1272-1317 (65.5%) 1360-1388 (29.9%)	1271-1389	91.77 ± 0.34	-25.4	-
R33	Agsu T1	W2	40.572	48.427	Plant Material	-150 ± 30	1954-1956 (95.4%)	-	101.88 ± 0.38	-29.0	-
R35	Agsu T1	W2	40.572	48.427	Charcoal	160 ± 30	1719-1786 (31.6%) 1906->1950(19.4%) 1832-1892 (17.9%) 1664-1708 (16.7%) 1792-1819 (9.8%)	1741-1948	98.03 ± 0.37	-25.6	-
R37	Agsu T1	U2	40.572	48.427	Charcoal	180 ± 30	1722-1814 (49.9%) 1656-1698 (19.2%) 1910->1950(19.0%) 1836-1880 (7.3%)	1650-1810	97.78 ± 0.37	-23.6	-
WG1	Water gap	-	40.559	48.236	Shell†	6040 ± 30	5026-4842 BC (95.4%)	-	47.15 ± 0.18	-7.8	-2.23

[1]All samples pretreated with acid/alkali/acid washes unless otherwise noted.
*Acid wash pretreatment only

†Acid etch pretreatment only

[2]All calibrations were done with OxCal v4.4 using the IntCal 20 curve.

489